Bulletin of Volcanology (2024) 86:95
https://doi.org/10.1007/s00445-024-01779-9

RESEARCH ARTICLE

# Quantification of volcanic degassing and analysis of uncertainties using numerical modeling: the case of Stephanos crater (Nisyros Island, Greece)

**Silvia Massaro[1,2] · Giancarlo Tamburello[2] · Giulio Bini[2] · Antonio Costa[2] · Manuel Stocchi[1] · Franco Tassi[3,4] · Rebecca Biagi[3] · Orlando Vaselli[3,4] · Giovanni Chiodini[2] · Fabio Dioguardi[1,5] · Jacopo Selva[6] · Laura Sandri[2] · Giovanni Macedonio[7] · Stefano Caliro[7] · Georges Vougioukalakis[8]**

Received: 5 April 2024 / Accepted: 24 October 2024


## Abstract

Nisyros Island (Greece) is affected by widespread gas emissions from fumarolic fields located at the bottom of hydrothermal craters in the southern part of its caldera. This morphology and the current low gas fluxes make Nisyros an ideal site for testing the limits of physics-based gas dispersal models in confined and low-emission conditions. Here, we focused our attention on the local scale volcanic gas dispersion from the Stephanos hydrothermal crater. In April 2023, a 1-week survey was carried out to measure weather data, $CO_2$ and $H_2S$ gas fluxes, air concentrations from portable gas stations, and chemical composition of fumarolic gases and to acquire thermal images of the crater floor. These data were used as inputs and boundary conditions for numerical simulations using a DISGAS-2.6.0 model in order to quantify the present-day volcanic degassing and its associated uncertainties, accounting for the meteorological variability. Model results are provided in terms of $H_2S$ probabilistic exceedance and persistence maps, showing gas concentrations within the crater that fall below the thresholds indicated for the occurrence of serious respiratory problems. Since DISGAS-2.6.0 does not account for chemical reactions, this study represents a good opportunity to discuss the methodological limits of simulating the dispersion of $H_2S$ which is challenging due to its rapid degradation and dilution in the atmosphere. In this regard, we also provided an empirical law of the $H_2S$ depletion in low-emission conditions that takes into account the uncertainties related to the field measurements.

**Keywords** Volcanic degassing · Carbon dioxide · Hydrogen sulfide · Probabilistic concentration maps

## Introduction

Much of the present-day knowledge about the degassing of natural systems comes from studies on persistently active volcanoes (e.g., Etna, Italy; e.g., Allard et al. 1991; Nyiragongo, Congo; e.g., Arellano et al. 2017; Ambrym, Vanuatu; e.g., Allard et al. 2006; Kīlauea, USA; e.g., Kern et al. 2020; Masaya, Nicaragua; e.g., van Manen et al. 2014; Erta Ale, Ethiopia; e.g., Boucher et al. 2018). These have, besides water vapor, carbon dioxide ($CO_2$) as one of the most

Editorial responsibility: A. Tadini

✉ Silvia Massaro
silvia.massaro@uniba.it

[1] Dipartimento di Scienze della Terra e Geoambientali, Università degli Studi "Aldo Moro", Bari, Italy

[2] Istituto Nazionale di Geofisica e Vulcanologia - Sezione di Bologna, Bologna, Italy

[3] Dipartimento di Scienze della Terra, Università degli Studi di Firenze, Florence, Italy

[4] Consiglio Nazionale delle Ricerche - Istituto di Geoscienze e Georisorse, Florence, Italy

[5] British Geological Survey, The Lyell Centre, Edinburgh, UK

[6] Dipartimento di Scienze della Terra, dell'Ambiente e delle Risorse, Università degli Studi "Federico II", Naples, Italy

[7] Istituto Nazionale di Geofisica e Vulcanologia - Osservatorio Vesuviano, Naples, Italy

[8] Hellenic Survey of Geology and Mineral Exploration, Athens, Greece

Published online: 26 November 2024

abundant magmatic volatiles, together with sulfur dioxide ($SO_2$) (e.g., Symonds 1994).

During quiescent periods, magmatic gases may be released from volcanic systems via diffusive soil degassing (e.g., Granieri et al. 2003; Chiodini et al. 2004) and fumarolic discharges (e.g., Solfatara, Campi Flegrei, Chiodini et al. 2001; Piton de la Fournaise, Reuniòn Island, Toutain et al. 2002; Furnas, Azores archipelago, Viveiros et al. 2012).

While $CO_2$ in soils and air behaves conservatively over relatively long periods, the atmospheric distribution and concentration of hydrogen sulfide ($H_2S$), mainly produced by $SO_2$ reduction in hydrothermal environments, are affected by weather conditions (e.g., Watson et al. 1978; Rickard and Luther 2007). Although the main sink of $H_2S$ in the atmosphere is the reaction with "OH" radicals (e.g., Watts 2000), other minor sinks can be found on a local scale, during and subsequent to rainfall events (Kristmannsdottir et al. 2000, Thorsteinsson et al. 2013) or due to reaction in lakes, soils, and vegetation (Bussotti et al. 1997; Cihacek and Bremner 1990). However, these interactions typically do not have first-order control. For example, Olafsdottir et al. (2014) conducted ad hoc measurement campaigns in Iceland showing that the depletion of $H_2S$ from the atmosphere is insignificant compared to the emissions within a 35 km distance from the sources.

Prolonged volcanic gas emission may produce acidification of soil, pollution of water, impinge on livestock, and fisheries and affect animal and human health (e.g., Baxter 1990; Baxter and Kapila 1989; Cronin and Sharp 2002; Costa et al. 2005; Linhares et al. 2015; Carapezza et al. 2023) even at very low concentration (< 1 ppm; ATSDR 1999; U.S. EPA 2003). Fatal consequences from sudden and violent volcanic gas emissions were also documented during limnic eruptions (Folch et al. 2009). The most famous example comes from the 1986 catastrophic event at Lake Nyos (Cameroon) where a $CO_2$ cloud was suddenly released, leading to the deaths of about 1700 people (e.g., Costa and Chiodini 2015, and references therein).

Many other deaths occurred because of accumulations of $CO_2$ or $H_2S$ in low-lying areas as flows and clouds (e.g., Auker et al. 2013; Stewart et al. 2022). Recently, a fatal incident occurred in September 2017 at La Solfatara crater (Italy), when an Italian family fell into a pit (https://www.bbc.com/news/world-europe-41243134) and died after having inhaled volcanic gases (https://www.ilmattino.it/napoli/cronaca/solfatara_il_piccolo_lorenzo_morto_per_scattare_un_foto_alla_fangaia-3872912.html). The key characteristic of $CO_2$ hazard is that usually there is no warning or a perceivable sign of it (Edmonds et al. 2018). $H_2S$ is instead detected by the rotten eggs odor, and it can cause a wide range of breathing difficulties even at relatively low concentrations (e.g., Baxter et al. 1990; World Health Organization 2000; Guidotti 2010; Santana et al. 2022). It was responsible for at least 46 fatalities (since the early twentieth century) at Rotorua (New Zealand) and a number of volcanoes in Japan (i.e., Kusatsu-Shirane and Adatara volcanoes; Williams-Jones and Rymer 2015).

Gas dispersal is controlled by multiple variables such as source location and magnitude, wind and terrain conditions, and gas species composition. In the last few years, more attention has been paid to test the capabilities of dispersion models to either quantify the associated hazard assessment (Massaro et al. 2021; 2022; Rafflin et al. 2024) or indirectly estimate the unknown gas contribution of fumarolic fluxes (Viveiros et al. 2023).

In this study, we investigated the permanently active degassing area at the Stephanos crater, Island of Nisyros (Dodecanese, Greece), located within the southeastern sector of the Lakki Plain area (Fig. 1). Combining geochemical data and numerical modeling, we provided a new methodology to quantify the volcanic degassing and the associated uncertainties in order to better understand the potential health risks in areas characterized by a persistent exposure to volcanic gas emissions.

Precautionally, the local authorities have delimited the fumarolized and boiling pools (observed in the center of the crater in April 2023) areas by ropes, so that they cannot be approached by tourists.

In the following, we describe the volcanological context of the site, the methods to acquire the geochemical data during the April 2023 gas survey, and the modeling approach. In the "Results" section, we confirmed the capability of DISGAS-2.6.0 in capturing the order of magnitude of the observed degassing within the crater and in the very proximal areas. We further provided the model outputs in terms of probabilistic exceedance and persistence maps of $H_2S$ concentration based on the current degassing scenario, incorporating meteorological data from the ECMWF-ERA5 global model (Hersbach et al. 2018a, b) collected over the past 30 years. Finally, modeling limits, uncertainties of field measurements, and chemical aspects of the $H_2S$ degradation and dilution in the atmosphere were critically addressed in the "Discussion" section.

## Volc Volcanological context, hydrothermal activity, and gas origin

Nisyros is a calc-alkaline volcano formed during the Pliocene–Pleistocene in the southeastern part of the Aegean Volcanic Arc (Fig. 1a, b; Vougioukalakis 1993). Two eruptive cycles include the cone-building activity fed by basaltic andesitic and andesitic magmas, the caldera-forming explosive activity, rhyolitic phreatomagmatic eruptions, and extrusion of dacitic-rhyolitic domes and lava

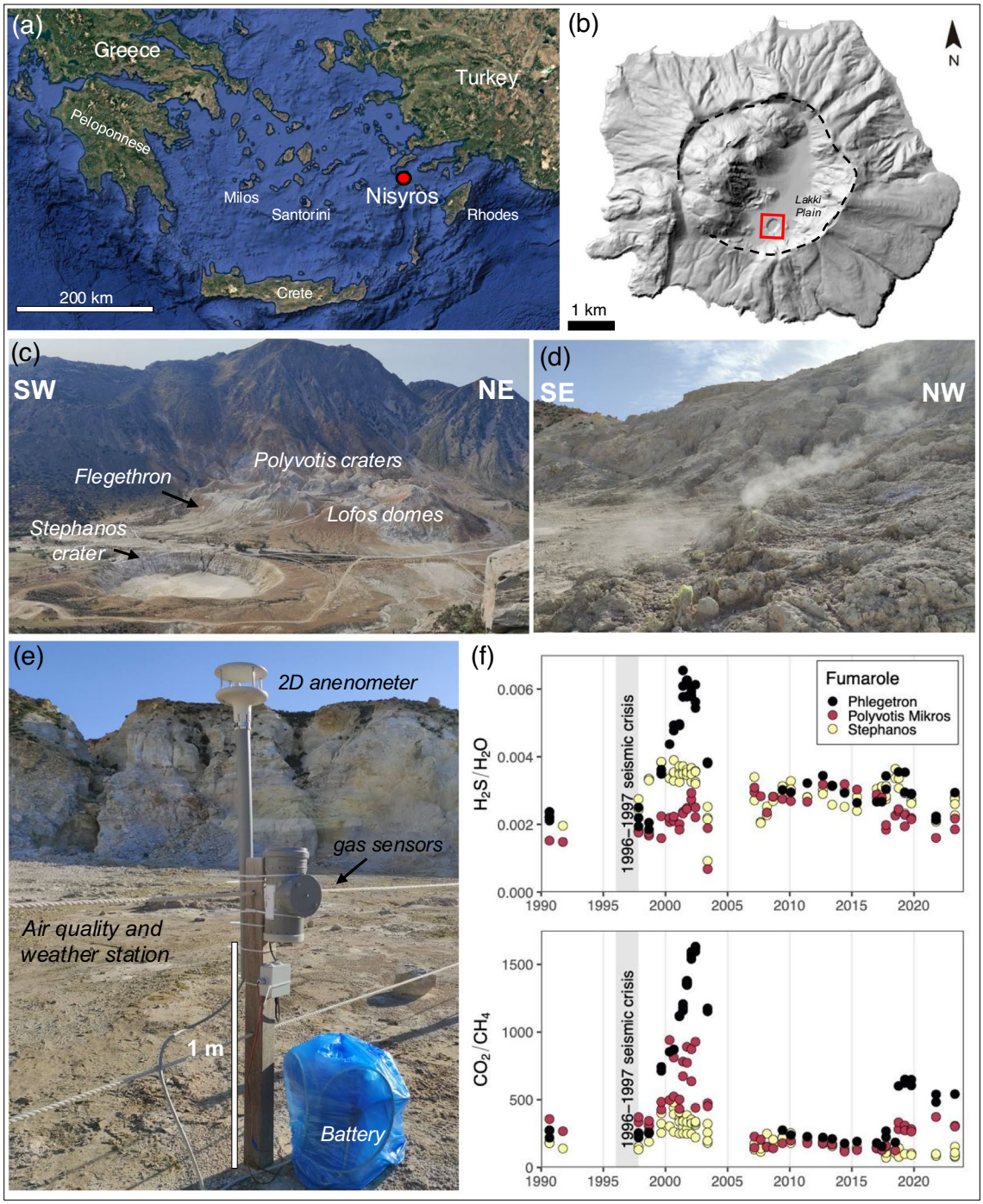


**Fig. 1** **a** Location of Nisyros Island in the Hellenic volcanic arc, Greece (©2023 Google); **b** 5 m resolution digital elevation model (DEM) of Nisyros (courtesy of HSGME). The red box included the investigated area. **c** Panoramic photo of the Lakki Plain area showing Stephanos crater, Flegethron, Polyvotis craters, and Lofos dome. **d** Fumarolic degassing from the inner wall of Stephanos crater during 20 April 2023. **e** Photo showing the 2D anemometer installed on the air quality station located in Stephanos crater at 1 m from the ground. **f** $H_2S/H_2O$ and $CO_2/CH_4$ molar ratios in fumarole gases collected from 1990 to 2023 (including those from this survey; after Bini et al. 2022)

flows. Since the last eruptions (about 20 ka; Popa et al. 2020), the volcanic activity has remained in a dormant stage, showing a large hydrothermal system expressed in fumaroles at boiling temperature of water and, at minor extent, thermal waters (e.g., Tibaldi et al. 2008; Dietrich and Lagios 2017).

Several hydrothermal eruptions occurred in the southern part of the caldera in historical times, concurrently with periods of enhanced seismicity. The last eruptions took place in 1871–1873 and 1887, generating the craters of Flegethron and Polyvotis (Marini et al. 1993, Fig. 1c). The largest crater is Stephanos (e.g., Marini et al. 1993; Fig. 1c), an elliptical crater (260 × 350 m, maximum depth 27 m) of unknown age, but probably prehistoric according to its well-preserved shape that seems to be affected by NE trending active faults and marked by an alignment of fumarolic vents (Dietrech and Lagios 2017).

During 1996–1997, a seismic crisis occurred (Papadopoulos et al. 1998) without culminating in any hydrothermal eruptions. However, the chemistry of fumarolic gases recorded a significant uprising of magmatic volatiles (e.g., a spike in the $CO_2/CH_4$ ratio, increasing trend of $H_2S/H_2O$ as shown in Fig. 1f) which caused pressure–temperature build-up in the hydrothermal system (Chiodini 2009; Bini et al. 2022).

Nisyros is one of the first volcanoes where soil $CO_2$ fluxes were measured (Brombach et al. 2001) and detailed maps of the degassing structures were identified (Caliro et al. 2005; Bini et al. 2019). Gases are emitted through the soil and fumarolic vents from the Stephanos, Flegethron, Kaminakia, Polyvotis craters, and Lophos domes and from fractures controlled by the regional tectonic faults-oriented NE-SW and NW–SE (Bini et al. 2019). The total soil $CO_2$ emission has not been high during the last 20 years (1999–2001: 81.6 ± 6.8 t $d^{-1}$; 2018: 100.6 ± 7.9 t $d^{-1}$; Bini et al. 2019 over a surveyed area of ca. 2.2 $km^2$) compared to other Mediterranean volcanoes (e.g., Solfatara of Campi Flegrei emits on average 1300 t $d^{-1}$ over a surveyed area of 1.4 $km^2$; Cardellini et al. 2017), but the hydrothermal system shows a large flux of energy which could increase during future unrests (e.g., Bini et al. 2019). The fumarolic gas discharges show outlet temperatures (96–100 °C) close to the boiling point of water at sea level and mainly consist of $H_2O$ followed by $CO_2$ and $H_2S$, while $N_2$, $H_2$, $CH_4$, CO, Ar, and He are minor components. The absence of strongly acid gases (i.e., $SO_2$, HCl, and HF) indicates that the fumarolic effluents are generated from a boiling hydrothermal reservoir rather than from direct magma degassing (Chiodini et al. 1993, 2007).

## Methods

### Diffusive gas flux

We estimated the $CO_2$ diffuse emission from the soil of the Stephanos crater during April 15–16, 2023 through 301 measurements carried out over a regularly spaced grid of 20 m × 20 m (Fig. 2a), using the accumulation chamber method (Chiodini et al. 1998). We used two fluxmeters manufactured by the University of Perugia and West Systems (Italy), which were intercalibrated by measuring given $CO_2$ concentration at increasing fluxes (Cardellini et al. 2003). To measure the soil $CO_2$ emission, the cylindrical chamber of the fluxmeter is placed on the soil, the soil gas enters the chamber, and it is pumped toward an infrared detector (LICOR LI-820 and LI-850). Eventually, the soil gas is reinjected into the chamber. The infrared detector records in real time the increase of the $CO_2$ concentration within the cylindrical volume, which is proportional to the soil $CO_2$ flux (in $gm^{-2}$ $d^{-1}$). To estimate the budget of $CO_2$ diffusively emitted into the atmosphere, we modeled the spatial continuity of the measured soil $CO_2$ fluxes, and then we fit the empirical variogram through weighted least-squares regression.

Then, we used this variogram model (spherical, nugget = 0.18, range = 175 m) to simulate the $CO_2$ fluxes at the unsampled locations of the investigated domain (5 m × 5 m) through sequential Gaussian simulations (sGs; see Cardellini et al. 2003, for further details). We constructed 1000 realizations and averaged the results in the center of each 5 m × 5 m cell of the domain. This geostatistical routine was performed using the package gstat (Pebesma 2004) of R (R Core Team 2023) providing a total diffusive $CO_2$ flux of ~ 25 t $d^{-1}$ (~ 0.28 kg $s^{-1}$; Fig. 2a). We remark that $H_2S$ is more soluble than $CO_2$ in water and is more likely to be dissolved in shallow aquifers during the upflow of gases toward the surface (Symonds et al. 2001). Furthermore, high diffusive emissions of $CO_2$ are often emitted into the atmosphere from areas characterized by soil temperatures close to the boiling point of water. This thermal anomaly reflects shallow steam condensation below the surface, facilitating the sequestration of more soluble gas species, such as $H_2S$ (Chiodini et al. 2005). For this reason, we assume the diffusive $H_2S$ from the soil is negligible.

### Fumarolic gas flux

At Nisyros, the gas emission from vents consists of relatively low-flux fumaroles dominated by water vapor, which are grouped within well-defined areas at the bottom of the hydrothermal eruption craters. The steam flux was measured from five selected fumaroles showing the highest fluxes and temperatures (the most vigorous ones) located at the bottom of the Stephanos crater (F1–F5 in Fig. 2b; Table 1), a very well-monitored area over time (see Chiodini et al. 1993; Marini and Fiebig 2005; Bini et al. 2022).

Attempts to measure low-flux fumaroles did not produce enough steam condensation to be measured. We used a properly designed stainless-steel funnel (Pecoraino et al. 2008) positioned upside down on the vents and cooled with water. Water vapor condensing from the fluids entering the funnel was collected and quantified. Such a steam flux, coupled with the gas/steam weight ratios analyzed in fumarolic fluids

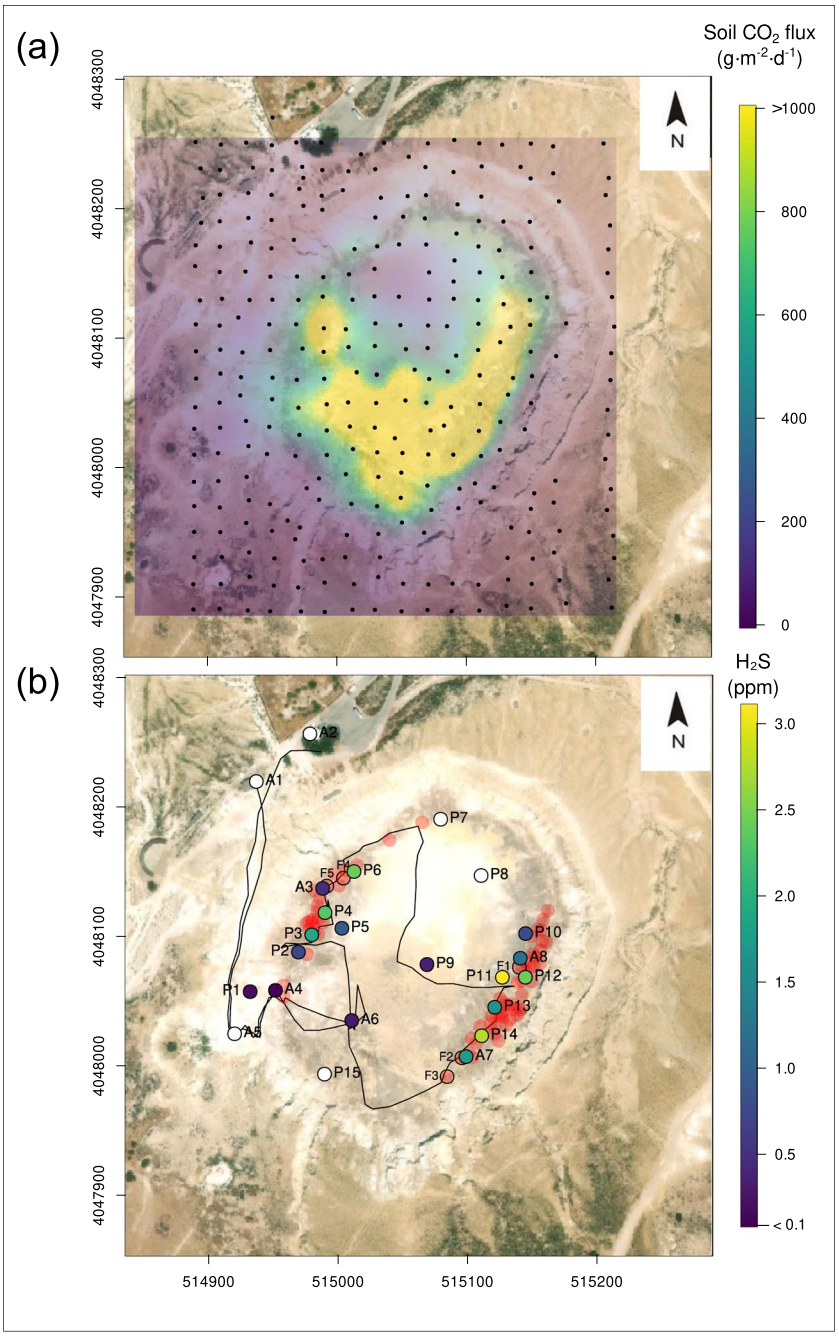


**Fig. 2** **a** Map of the diffusive $CO_2$ flux (~25 t $d^{-1}$) emitted from Stephanos crater area built using sequential Gaussian simulations. **b** Locations of instantaneous $CO_2$ and $H_2S$ concentration (ppm) collected at ~ 1 m from the ground during April and June 2023 (Table 2). The black line indicates the pathway of the MG measurements. In red are the positions of the 73 active fumaroles along the inner wall of the crater observed during 18–22 April 2023. Maps coordinates are in Datum WGS84 (Projection UTM 35N)

**Table 1** Estimation of $H_2O$ flux from five fumaroles (F1–F5; Fig. 2b) converted in $H_2S$ and $CO_2$ flux (t $d^{-1}$) and used to provide an averaged estimation considering the 73 active fumaroles within the crater (Fig. 3). The location of the samples are in Datum WGS84 (Projection UTM 35N)

| ID fumaroles | Coordinates (Easting, Northing in m) | | $H_2O$ (ml $d^{-1}$) | $H_2S$ (t $d^{-1}$) | $CO_2$ (t $d^{-1}$) |
|---|---|---|---|---|---|
| F1 | 515139.95 | 4048076.74 | 52,052 | $2.55 \cdot 10^{-4}$ | $1.56 \cdot 10^{-3}$ |
| F2 | 515095.52 | 4048006.89 | 49,159 | $2.41 \cdot 10^{-4}$ | $1.47 \cdot 10^{-3}$ |
| F3 | 515084.19 | 4047992.34 | 78,039 | $3.83 \cdot 10^{-4}$ | $2.34 \cdot 10^{-3}$ |
| F4 | 514991.33 | 4048139.27 | 15,136 | $7.41 \cdot 10^{-5}$ | $4.54 \cdot 10^{-4}$ |
| F5 | 514992.77 | 4048136.61 | 51,067 | $2.51 \cdot 10^{-4}$ | $1.53 \cdot 10^{-3}$ |
| *Average flux:* | | | | $2.4 \cdot 10^{-4}$ | $1.47 \cdot 10^{-3}$ |
| *Standard Dev:* | | | | $1.1 \cdot 10^{-4}$ | $6.71 \cdot 10^{-4}$ |

(i.e., $H_2S/H_2O$, $CO_2/H_2O$) collected through direct sampling techniques (see Vaselli et al. 2006, and Caliro et al. 2015, for further details), enabled us to compute the fumarolic flux of $H_2S$ and $CO_2$ shown in Table 1.

To this end, we used the averaged $H_2O$ flux from the five fumaroles (Table 1), multiplied by the averaged $H_2S/H_2O$ weight ratio of ~ 0.0049 to get a representative averaged $H_2S$ flux for a single fumarole of ~ 2.4 $10^{-4}$ t $d^{-1}$ (~ $2.8 \cdot 10^{-6}$ kg $s^{-1}$).

In order to assess the total number of fumarolic gas sources, thermal images of the crater floor were acquired from the northern rim (Fig. 3a, b). Fumaroles were identified as temperature maxima in the thermal image, which varied from ~ 20 up to ~ 50 °C (Fig. 3c, d). Such temperatures were lower than those measured with a thermocouple during fumarolic gas sampling (~ 100 °C). This discrepancy may be due to (i) a low resolution of the thermal sensor averaging the temperature over a large emissive surface and (ii) the temperature referred to the outermost portion of the shallow rock/soil.

To identify the threshold peak temperature above which we consider the point to be a fumarole, we plotted the number of identified fumaroles at different threshold temperatures. Our objective was to minimize the residual standard error (RSE) of the two best-fit lines in order to identify the threshold temperature at which fumarole counts exhibited a slower rate of decrease. We chose 30 °C as the threshold temperature value, above which we referred to the "flattening" of the fumarole count (Fig. 3e).

Since we measured the fluxes from the strongest fumaroles and associated their fluxes with minor fumaroles observed during the mapping, such an estimate should be considered a maximum estimate. The total number of detected fumaroles ($n = 73$; 24 to the west and 49 to the east) was then multiplied by the averaged $H_2S$ flux for a single fumarole to get the total averaged $H_2S$ fumarolic flux of ~ $1.8 \cdot 10^{-2}$ t $d^{-1}$ (~ $2.0 \cdot 10^{-4}$ kg $s^{-1}$) within the crater. Using the same approach, we obtained the averaged fumarolic $CO_2$ flux of ~ 0.43 t $d^{-1}$ (~ $5.0 \cdot 10^{-3}$ kg $s^{-1}$), considering the averaged $CO_2/H_2O$ weight ratio of ~ 0.03.

## Acquisition of wind data and $CO_2$ and $H_2S$ concentrations from the gas stations

A Delta Ohm HD53LS 2-axis ultrasonic static anemometer was installed on station S4 at ~ 1.5 m from the ground (Fig. 1e), to measure wind speed, direction (U-V Cartesian

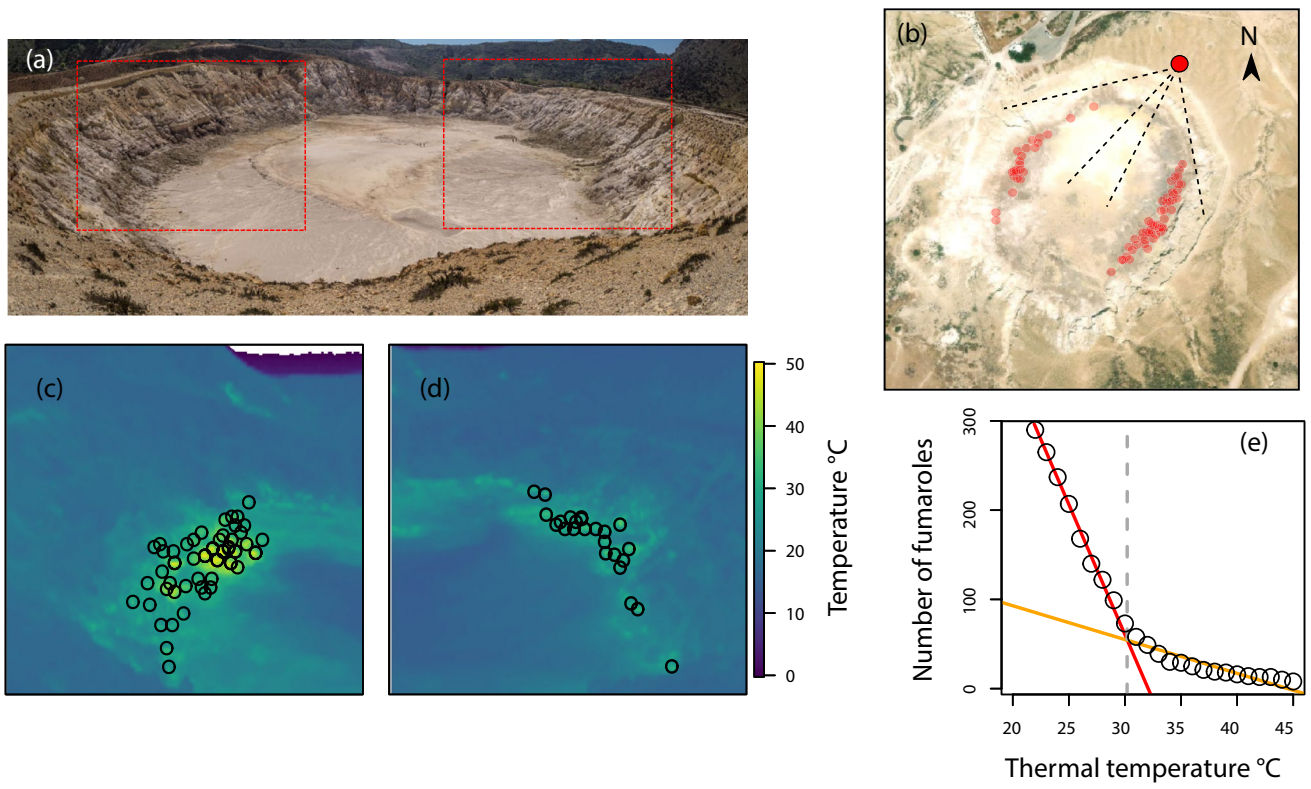


**Fig. 3** **a** Photo of the Stephanos crater floor indicating two areas (red boxes) where the most active fumarolic degassing has been assessed during 18–22 April 2023. **b** Field of view (FOV) of the 73 active fumaroles identified by the thermal images of the crater floor (**c**, **d**) indicating the emission sources (black dots) having temperatures between 20 and 50 °C. **e** graph plotting the number of identified fumaroles at different threshold temperatures

components of wind speed), and wind gust with an acquisition rate every 15 s (Supplementary Material). The low power consumption of the instrument allowed the installation with power from a 12-V battery for ~ 5 days.

$CO_2$ and $H_2S$ concentrations in the air were measured with three different methods: (i) portable infrared sensors installed on the gas stations, (ii) MultiGas (MG) analyzer, and (iii) bubblers (alkaline chemical traps).

(i) Four cost-effective gas stations developed by the University of Florence (Biagi et al. 2024; Fig. 1e) and equipped with diffusive sensors were assembled to continuously measure $CO_2$ concentrations in the ambient air surrounding the emitting sources from 18 to 22 April 2023 (Supplementary Material for technical details).

(ii) The MG analyzer (https://www.tecnosens.it/multisensor/multisensor-board) was equipped with a diffusive electrochemical $H_2S$ sensor (range, 0–100 ppm; maximum overload, 500 ppm; repeatability: < ± 2% $H_2S$ equivalent) and infrared $CO_2$ sensor (range, 0–5000 ppm; repeatability, < ± 2% $CO_2$ equivalent) that were used to measure the air gas concentrations along multiple transects (at different distance from the fumaroles, Fig. 2b).

The response time (T90) for the $CO_2$ and $H_2S$ sensors are < 30 and < 25 s (at 20 °C), respectively. This T90 difference generates a delay of a few seconds between the $CO_2$ and $H_2S$ concentration time series that has been corrected by cross-correlation. Then, we calculated the volcanic $CO_2/H_2S$ molar ratio following the method described in Tamburello (2015).

(iii) The third employed methodology enabled us to calculate instantaneous gas concentrations at ~ 1 m from the ground by bubbling the air in 25 ml of a 4 M NaOH and 0.15 M $Cd(OH)_2$ trap (Montegrossi et al. 2001) with a portable pump with a flux of 200 cc/min. Air samples were collected in 23 sites (Fig. 2b) within Stephanos crater during the April 2023 survey and June 2023. Both $CO_2$ and $H_2S$ are reactive species, which were absorbed in the alkaline solution. $H_2S$ was trapped by precipitating as CdS, and the concentrations were analyzed by ion chromatography (Metrohm 761 Advanced Compact IC) after converting sulfide to sulfate through the addition of $H_2O_2$ and dissolving the solid phase in a solution of 10 ml solution of ultrapure water (resistivity of 18.2 MΩ.cm at 25 °C, Milli-Q) and 0.025 g NaOH in pellets (Montegrossi et al. 2001). The $CO_2$ content, dissolved in the liquid phase, was determined through acidimetric titration. The values of $H_2S$ and $CO_2$ concentrations at the sample points are reported in Table 2.

**Table 2** Instantaneous $CO_2$ and $H_2S$ concentration (ppm) measured with the bubblers within Stephanos crater during April (A1–A8) and June 2023 (P1–P15) at ~ 1 m from the ground (Fig. 2b). The $CO_2$ background (ca. 415 ppm) is included. Map coordinates are in Datum WGS84 (Projection UTM 35N)

| Period | Sample points | Coordinates (Easting, Northing in m) | | $CO_2$ (ppm) | $H_2S$ (ppm) |
|---|---|---|---|---|---|
| April 2023 | A1 | 514937.70 | 4048218.27 | 420 | < 0.1 |
| April 2023 | A2 | 514980.13 | 4048255.17 | 451 | < 0.1 |
| April 2023 | A3 | 514988.83 | 4048135.83 | 568 | 0.48 |
| April 2023 | A4 | 51454.17 | 4048057.78 | 495 | 0.11 |
| April 2023 | A5 | 514922.91 | 4048024.23 | 415 | < 0.1 |
| April 2023 | A6 | 515011.20 | 4048034.81 | 550 | 0.31 |
| April 2023 | A7 | 515099.82 | 4048006.68 | 623 | 1,6 |
| April 2023 | A8 | 515142.09 | 4048082.18 | 590 | 1.1 |
| June 2023 | P1 | 514932.21 | 4048057.99 | 471 | 0.21 |
| June 2023 | P2 | 514969.46 | 4048088.25 | 511 | 0.69 |
| June 2023 | P3 | 514979.74 | 4048101.60 | 622 | 1.7 |
| June 2023 | P4 | 514990.027 | 4048118.76 | 650 | 21 |
| June 2023 | P5 | 515002.993 | 4048106.67 | 554 | 0.89 |
| June 2023 | P6 | | 4048150.49 | 630 | 2.2 |
| June 2023 | P7 | 515079.19 | 4048190.86 | 425 | < 0.1 |
| June 2023 | P8 | 515110.43 | 4048147.40 | 415 | < 0.1 |
| June 2023 | P9 | 515068.64 | 4048078.76 | 490 | 0.36 |
| June 2023 | P10 | 515144.74 | 4048102.57 | 523 | 0.75 |
| June 2023 | P11 | 515126.80 | 4048069.08 | 642 | 2.8 |
| June 2023 | P12 | 515144.57 | 4048069.11 | 610 | 2.2 |
| June 2023 | P13 | 515120.92 | 4048045.94 | 590 | 1.5 |
| June 2023 | P14 | 515110.86 | 4048023.88 | 633 | 2.5 |
| June 2023 | P15 | 514936.97 | 4047994.30 | 420 | < 0.1 |

## Numerical modeling

The atmospheric dispersion of $CO_2$ emitted from the crater soil and fumaroles was modeled through DISGAS v2.6.0 (Costa and Macedonio 2016), a 3D Eulerian dilute gas dispersion model, which solves the advection–diffusion equation.

DISGAS is coupled with DIAGNO, a diagnostic wind simulator (Douglas et al. 1990) to provide a quasi-steady-state gridded wind field in the computational domain. This model adjusts the domain-scale mean wind for kinematic terrain effects and then calculates a new wind field with a divergence minimization to ensure mass conservation.

The passive condition is assumed to be governed by the wind and atmospheric turbulence that it is legitimate for diluted gases (see Costa et al. 2005; Costa and Macedonio 2016). The validity of such a passive approximation can be assessed by estimating the Richardson number (Britter and McQuaid 1988; Cortis and Oldenburg 2009; Costa et al. 2013) of the emission source:

$$Ri = \frac{1}{v^2}\left(\frac{g'q}{R}\right)^{\frac{2}{3}} = \frac{\sqrt[3]{\frac{g^2(\rho_g-\rho_a)^2}{\rho_a^2}q^2}}{v^2R^{\frac{2}{3}}} \quad (1)$$

where $g'$ is the apparent gravity acceleration; $\rho_g$ and $\rho_a$ are the air and the gas densities, respectively; $q$ is the volumetric flow rate; $R$ is the plume size (e.g., plume radius); and v is the wind velocity at the reference altitude (i.e., 10 m). For $Ri < 0.25$, transport is substantially passive, whereas for $R_i > 1$ is mainly density-driven (Cortis and Oldenburg 2009; Costa et al. 2013).

We validated the passive approximation with the Richardson number (Eq. 1). Considering the $CO_2$ diffusive flux of ~ 25 t $d^{-1}$ (~ 0.28 kg $s^{-1}$), a reference plume radius of ~ 300 m (as approximation of the radius of the crater, which is where the diffuse degassing occurs), a $CO_2$ density of ~ 1.45 kg $m^{-3}$ (at $T = 100$ °C, and $P = 1013$ mbar) and air density of ~ 1.2 kg $m^{-3}$ (at standard conditions), we get Ri ≈ 0.012. Considering the fumarolic $CO_2$ flux of ~ 0.43 t $d^{-1}$ (~ $5.0 \cdot 10^{-3}$ kg $s^{-1}$) emitted in typical wind conditions (~ 1 m $s^{-1}$ as a mean of typical wind velocities during the day and night measured with our anemometer), a reference plume radius of ca. 6 m (as seen from the active fumaroles within the crater) and a $CO_2$ density of ca. 1.28 kg $m^{-3}$ (at $T = 150$ °C, and $P = 1013$ mbar), we get Ri ≈ 0.005. In both cases, the dispersion can be assumed passive. To provide the probabilistic outputs, we used VIGIL-v1.3.5 workflow (Dioguardi et al. 2022), a Python tool interfaced with both passive (DISGAS v2.6.0) and dense gas (TWODEE-2 v2.6.0; Folch et al. 2009) flow models. The workflow has three stages that must be run sequentially. These can be run in parallel, saving high computational times to run the simulations for probabilistic volcanic hazard assessment applications. At the beginning, DIAGNO starts to generate time-dependent terrain-adapted wind fields from either user-provided or retrieved data by the ECMWF-ERA5 global model (Hersbach et al. 2018a,b). Since the ERA5 data refer to grid points with a spatial resolution of 0.25° (~ 30 km) and the typical domain of simulations run by VIGIL has dimensions of hundreds of meters to a few km, the data are linearly interpolated onto the midpoint of the computational domain and furnished to the DIAGNO module. In our case, to model the $CO_2$ concentration at specific tracking points, we assumed $CO_2$ the main tracking species given that we inferred the total $CO_2$ flux (Fig. 2). Additionally, we remark that $CO_2$ has a low solubility in water and hence is almost entirely emitted into the atmosphere (Chiodini et al. 2005). For this reason, the effect of condensation on $CO_2$ can be considered negligible.

Hence, the outputs yield concentrations expressed values in excess of background $CO_2$ levels in the air at heights selected by the user. Consequently, to model $H_2S$ concentration, we assumed $H_2S$ as the main tracked species using as input data the estimated fumarolic $H_2S$ flux described above. We then provided the probabilistic exceedance maps posed by $H_2S$ dispersion considering the meteorological variability of the past 30 years (1993–2023). In order to get a robust statistical similarity, wind profiles of 1000 days were randomly sampled from the ECMWF-ERA5 dataset and automatically downloaded by VIGIL-1.3.5 in GRIB format with a 1-h temporal resolution. The computational domain was set to a square area of 600 × 600 m with a horizontal resolution of 5 m. A 5-m resolution DEM (courtesy of HSGME) was used as topography. All the simulations were run and stored at the ReCaS DataCenter of the University of Bari and the National Institute of Nuclear Physics (https://www.recas-bari.it/index.php/it/).

## Results

We run a single simulation from April 18 to 22, 2023, using the local wind conditions acquired from the 2D anemometer (Fig. 1e; Supplementary Material) to reproduce the order of magnitude of the observed volcanic degassing for $CO_2$ and $H_2S$, respectively.

As input data, we used the total amount of $CO_2$ flux composed by the diffusive of ~ 25 t $d^{-1}$ and the fumarolic contribution of ~ 0.43 t $d^{-1}$. Regarding $H_2S$, we used the fumarolic flux of ~ 1.8 $10^{-2}$ t $d^{-1}$.

Five tracking points (T1–TP5) corresponding to the installed air quality gas stations were selected. For each point, we built the ECDF of the simulated average of $CO_2$ and $H_2S$ concentration at 1 m from the ground (Fig. 4). This stepwise function represents the proportion of observations

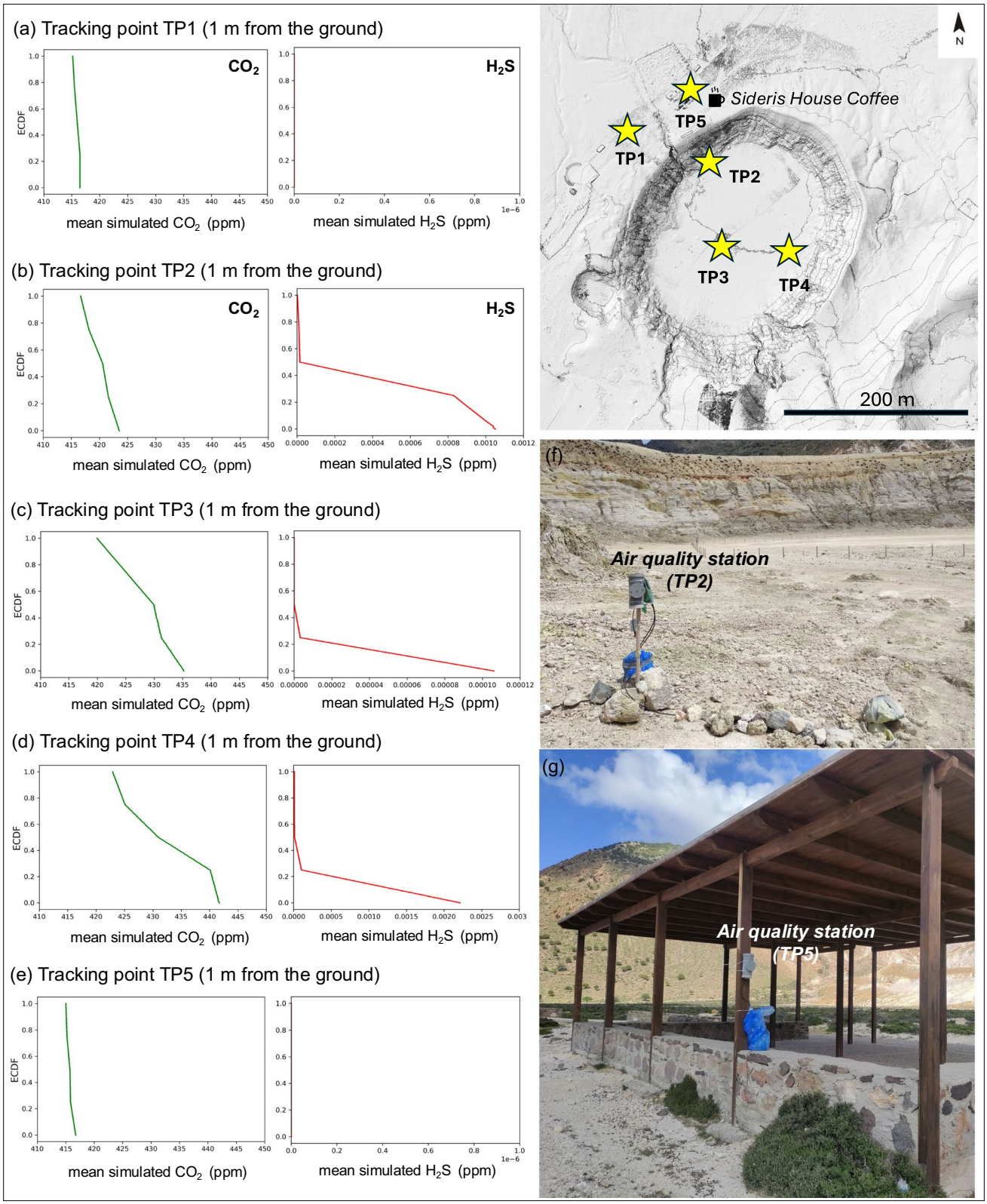


**Fig. 4** ECDFs of the mean $CO_2$ and $H_2S$ concentration from April 18 to 22, 2023, at 1 m from the ground corresponding to the air quality stations (yellow stars) corresponding to the tracking points: **a** TP1 (514933.77, 4048212.71), **b** TP2 (515002.93, 4048160.14), **c** TP3 (515010.39, 4048031.70), **d** TP4 (515095.35, 4048050.34), and **e** TP5 (514985.12, 4048264.27). The simulations were run using the local weather data acquired by the 2D anemometer (corresponding to TP4; Fig. 1e). The calculated value of the $CO_2$ background is 415 ppm. The location of the tracking points are in Datum WGS84 (UTM 35N)

that fall below a given value, providing a visual representation of how values are distributed at that location over time. It shows, for each value on the *x*-axis, the probability that observations at the point are less than or equal to that value.

The ECDFs of the simulated average of $CO_2$ show a negligible value (< 5 ppm) over the background value (~ 415 ppm) outside the crater (TP1 and TP5; Fig. 4a, e, and g) reaching a slight increase within the crater (~ 10–20 ppm; TP2-3–4; Fig. 4b, c, d, and f). This qualitative comparison highlighted that $CO_2$ is very far from posing a hazard to human health (Table 3). The simulated average of $H_2S$ concentration is ~ 0 ppm outside the crater (TP1–TP5; Fig. 4a, e, and g) and negligible at TP3 (< 0.0001 ppm; Fig. 4c). Slightly higher values can be observed at tracking points 2 (< 0.001 ppm; Fig. 4b) and 4 (< ~ 0.002; Fig. 4d).

Figure 5 reports the long-term probabilistic exceedance maps posed by $H_2S$ dispersion, merging 1000 runs. It is worth noting that the exceedance probability at a point is simply 1 - ECDF (value at that point). For example, if a location has an ECDF value of 0.9 for a particular concentration, this implies that 90% of the time, the concentration is below or equal to that value, and therefore, the exceedance probability is 10%, meaning the concentration will exceed this threshold in 10% of cases.

The maps indicate the daily averaged $H_2S$ concentration field at 1.5 m above the ground (the typical breathing height of adult humans) at three selected exceedance probabilities: 10% as generally employed in Bayesian Event Tree models, 16% equivalent to $1\sigma$ level of uncertainty, and 50% as the mean. The $H_2S$ dispersion is within the crater ranging from 0.002 ppm to a peak value of ~ 0.15 ppm at 10%, ~ 0.14 ppm at 16%, and ~ 0.07 ppm at 50% of exceedance probability, only when closely approaching the active fumaroles.

**Table 3** Threshold limits, principal effects, and exposure time for ambient air $H_2S$ concentration. *TWA* time-weighted average, measure used to assess the average exposure to a substance over a specified period, usually an 8-h workday. *STEL* short-term exposure limits, usually 15 min

| $H_2S$ thresholds | Effect for human health | Exposure time | References |
|---|---|---|---|
| **0.0036 ppm** | No effects reported | 1 year in Iceland | Olafsdottir et al. (2014) |
| **0.005–0.01 ppm** | Level at which the general population is protected from eye irritation or odor | From 30 min to 24 h | WHO (1981) |
| **0.025 ppm** | No effects reported | 1-h limit in Hawaii | State of Hawaii (2002) |
| **0.02 ppm** | Level at which human exposure is likely to be without appreciable adverse health effects | 15 days–1 year | Agency for Toxic Substances and Disease Registry (ATSDR) (1999) |
| **0.03 ppm** | Odor threshold (highly variable) | 24-h running average in Iceland<br>1-h limit in California | Olafsdottir et al. (2014)<br>www.arb.ca.gov |
| **0.2–0.65 ppm** | Risk of cataract and eye irritation | | WHO (2000) |
| **0.7–1 ppm**<br>**1 ppm**<br>**< 2 ppm** | Acute eye damage and respiratory irritation<br>Dangerous consequences in asthmatic people | 8-h occupational exposure in Italy | WHO (2000) |
| **5 ppm** | Moderate offensive odor may be associated with nausea, headaches, tearing of the eyes | 8-h occupational exposure in Iceland and Europe (TWA)<br>1-h limit average in New Zealand (not in geothermal areas) | Guidotti (2010)<br>European Union (2009)<br>Olafsdottir et al. (2014)<br>www.mfe.govt.nz |
| **10 ppm**<br>**15 ppm*** | | 8-h occupational exposure limit in Alberta<br>15-min occupational exposure limit in Iceland and Europe (STEL)<br>*15-min occupational exposure limit in Alberta | U.S. Environmental Protection Agency (U.S.EPA) (2003); European Union (2009)<br>Guidotti (2010) |
| **10.8–35.9 ppm** | Acute ocular, respiratory, muscular pathologies | | WHO (2000) |
| **20–50 ppm** | Conjunctivitis (eye irritation) and lung irritation. Possible eye damage after several days of exposure | | Guidotti (2010) |
| **100 ppm** | Immediate danger to healthy people (e.g., olfactory paralysis) | | WHO (2000) |
| **> 500 ppm** | Immediate danger to healthy people | Instantaneous | WHO (2000) |

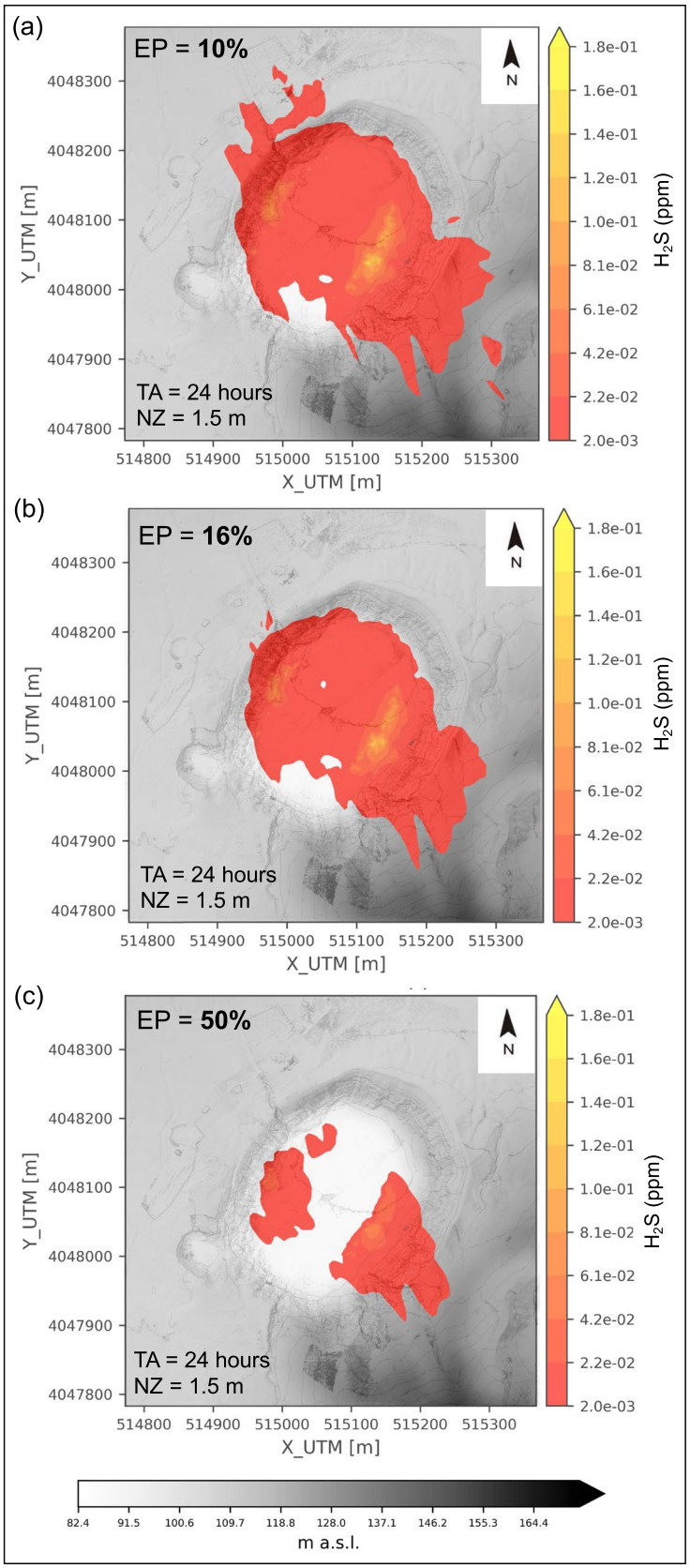


**Fig. 5** **a** Long-term probabilistic $H_2S$ concentration maps considering 1000 days of wind profiles randomly sampled from the ECWMF-ERA5 global model from 1993 to 2023. The daily averaged concentration values (ppm) are referred to 1.5 m from the ground with the exceedance probability of **a** 10%, **b** 16%, and **c** 50%

## Discussion

### Analysis of the probabilistic gas dispersion and health impacts

The probabilistic outputs shown in Fig. 4 indicate that there is no hazard posed by $CO_2$ and $H_2S$ outside the crater, as well as no serious conditions are expected to occur within it, considering the present-day volcanic degassing. Our simulated averaged concentrations result to be lower than those reported in the literature for the same investigated area (see Gagliano et al. 2019) and are in very good agreement with the instantaneous concentrations acquired during the April–June 2023 (Fig. 2b; Table 2) and the $CO_2$ concentration time series measured by the gas sensors during the gas survey (Supplementary Material).

The probabilistic $H_2S$ concentration maps shown in Fig. 5 indicate a worse occurrence (i.e., 10% of exceedance probability) of the averaged concentration field up to ~ 0.15 ppm only in the proximity of the active fumaroles, considering a long-term series of reanalysis weather data which statistically cover the seasonal effect of winds variability over the island. However, the maps do not explore the full variability of the input parameters since these are based on a single-degassing scenario defined by field measurements considering a fixed number of fumaroles, location, and an averaged $H_2S$ gas flux. These variables can vary in time, but a robust estimation of the total number of active fumaroles during the April 2023 gas survey ($n = 73$) has been assessed despite the variability of the coefficients of reflectivity, emitted temperature, and actual distance. We are interested in a relative threshold value, and this would not change the number of identified fumaroles (Fig. 3).

$H_2S$ poses an immediate danger to healthy people at very high concentrations (> 100 ppm), but some guidelines indicate that dangerous consequences can also occur at concentrations from 0.02 to 2 ppm in asthmatic individuals (Table 3). Using the 1000 model results, we calculated the probabilistic $H_2S$ persistence which indicates the fraction of time during a day in which the $H_2S$ concentration persists in the atmosphere. In Fig. 6, we show the long-term persistence maps showing the probability of exceeding a specific concentration threshold during an exposure time (set by the user, according to the odor nuisance and health impacts set in different countries; Table 3) which can be continuous or discontinuous throughout the day. In this way, it is possible to know how often, across all the simulations, the gas concentration thresholds are exceeded, based on a robust statistics of meteorological conditions (i.e., 30 years). For computational reasons, the minimum temporal resolution considered in the simulations is 1 h.

Considering that this area is daily visited by tourists almost over the entire year (e.g., Dietrich and Lagios 2017), in Fig. 6a, we show the probability of overcoming values of 0.03 ppm for 1 h (considering this a reasonable maximum time to visit the crater), which is significantly high (up to 100%) close to the crater rim in the eastern and western sectors. We selected such a threshold value following Lambert et al. (2006) that, for short-term exposure, suggests 25 ppb (~ 0.03 ppm) of $H_2S$ as the lowest concentration capable of causing eye irritation.

In Fig. 6b, we show the map using a $H_2S$ concentration threshold of 0.01 ppm for an exposure time of 24 h (Table 3). Also, in this case, the highest probabilities are found in the eastern and western sectors of the crater rim. This implies that these areas are almost constantly affected by non-negligible levels of $H_2S$ which, for shorter intervals, can overcome 0.03 ppm. Such conditions may represent a hazard for people affected by pre-existing respiratory problems and/or distress to healthy individuals (e.g., nausea, headaches, tearing of the eyes) in case of calm wind conditions.

It is worth noting that after the volcanic unrest occurred during the 1996–1997 seismic crises, both the seismicity and the chemical composition of fumarole gases returned to pre-crisis values, and currently Nisyros caldera appears to be in a dormant stage, characterized by a low degassing activity (e.g., Bini et al. 2022). Bini et al. (2022) hypothesized that the last episode of magmatic degassing during the unrest (1996–1997) occurred from a mature, silicic reservoir, whose presence was also consistent with the evolved products erupted in the last ~ 100 ka at Nisyros (Popa et al. 2019; 2020). These eruptions are thought to have been triggered by mafic magma recharges in the shallow mature reservoir below the caldera (Popa et al. 2019). Currently, there are no signs of more primitive gases that could recharge the system, and a forthcoming eruptive activity thus appears unlikely. This supports the idea that over a long-time scale, the total gas emission might be similar to that estimated today. However, new episodes of magmatic degassing are able to pressurize the hydrothermal system and cause a variation in the chemistry of gas emission, and an increase of their fluxes cannot be excluded.

### Modeling limits and $H_2S$ degradation in the atmosphere

The results presented in this study confirm DISGAS-2.6.0 as a tool for an improved understanding of the atmospheric and environmental impacts of the low $H_2S$ degassing from the Stephanos crater but also its potential for reliable prediction in case of unexpected events. However, the quantification of volcanic degassing and its associated uncertainties are strictly affected by the limits of the numerical modeling and

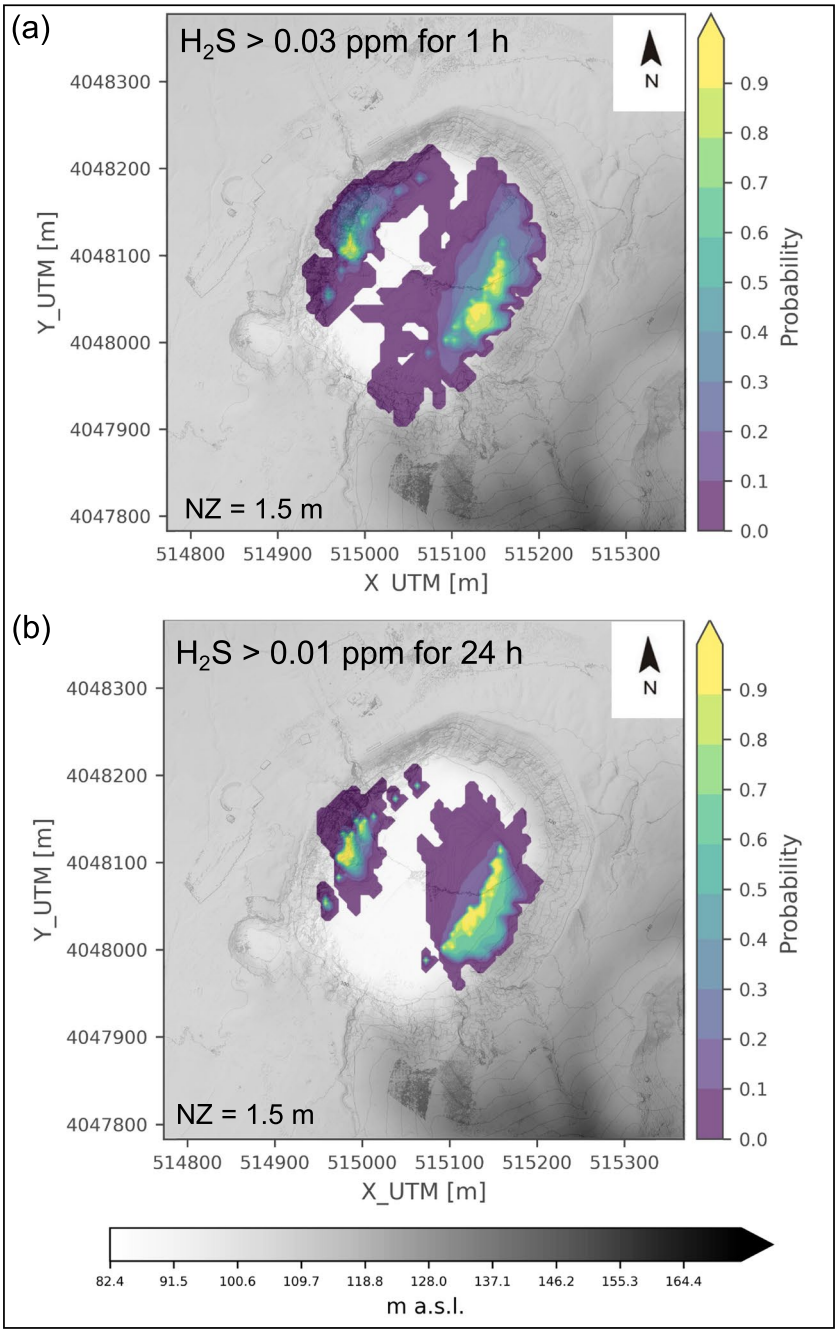


**Fig. 6** Long-term probabilistic persistence maps indicating the probability to reach $H_2S$ concentrations greater than **a** 0.03 ppm in 1 h and **b** 0.01 ppm in 24 h at 1.5 m from the ground, according to the threshold limits set by different countries and organizations (Table 3)

the field measurements that have to be taken into account in this analysis.

DISGAS-2.6.0 is a physics-based model that does not account for chemical reactions. A chemical module able to account for the degradation of $H_2S$ (e.g., oxidation) at increasing distance from the source is essential to provide a more reliable reproduction of the concentration field in the atmosphere of such a reactive compound and has to be integrated in the next version of DISGAS.

In order to assess the extent of $H_2S$ degradation inside Stephanos crater, we carried out measurements of gas concentrations at different distances from the fumaroles. We measured $H_2S$ concentrations > 10 ppm at a few centimeters from the fumaroles (with the MG analyzer). Hence, we calculated the volcanic $CO_2/H_2S$ molar ratio (removing the atmospheric $CO_2$ background of ~ 415 ppm) at different values of $H_2S$ concentrations (ranging from 0.1 to 100 ppm). In conservative conditions, the fumarolic $CO_2/H_2S$ molar ratio (~ 3.3) should not change significantly during diffusion in the atmosphere. Instead, Fig. 7 shows that the $CO_2/H_2S$ molar ratio increases as $H_2S$ concentrations decrease. This effect is more evident at $H_2S$ concentrations below 20 ppm.

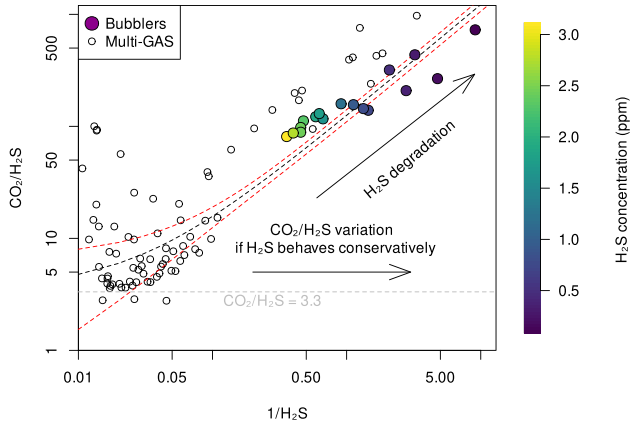


**Fig. 7** Diagram of the observed trend of the $CO_2/H_2S$ molar ratio vs. $1/H_2S$ concentration (ppm) estimated with MG and bubblers during the April 2023 gas survey

Our data (MG and bubblers) shows a $CO_2/H_2S$ asymptotic value of 3.55 for increasing $H_2S$ concentrations, very close to the composition obtained with the direct sampling where air dilution is negligible. The observed variation of the $CO_2/H_2S$ ratio with the concentration of $H_2S$ suggests that part of the $H_2S$ is lost due to oxidation processes occurring from the fumaroles to the measuring stations, as observed in other similar contexts by Badalamenti et al. (2001), Carapezza et al. (2003), and Biagi et al. (2022).

If we consider that the $H_2S$ degradation already occurs at only a few centimeters from the fumaroles and that at several meters $H_2S$ was below the detection limit of the bubblers (0.1 ppm), we argue that our modeled gas dispersion must be considered an overestimate. The real $H_2S$ concentrations in the air are certainly lower, minimizing the risk for visitors in the crater.

## Conclusions

This study represents an initial attempt to quantify the local-scale dispersion of volcanic gases from Stephanos crater (Nisyros, Greece) by integrating field measurements and numerical modeling, as well as a valuable opportunity to address the methodological constraints in simulating the dispersion of $H_2S$, which poses challenges due to its rapid degradation and dilution in the atmosphere.

Our results suggested that the DISGAS-2.6.0 model is able to reproduce the order of magnitude of the observed gas concentrations during the April 2023 gas survey. Although this model still does not account for chemical reactions, long-term probabilistic exceedance and persistence maps of $H_2S$ concentration were built using VIGIL-1.3.5 workflow considering a fixed degassing scenario but randomly varying the meteorological data over the last 30 years. The model outputs indicate that no serious health impacts can be addressed within Stephanos crater considering the present-day $H_2S$ gas fluxes. In order to take into account the effects related to the temporal and spatial loss of $H_2S$, a new empirical model of $H_2S$ depletion under low-emission conditions is also proposed, accounting for uncertainties associated with field measurements. A simplified flowchart of the adopted procedure is reported in Supplementary Material.

Finally, the proposed methodology can be applied to any other volcanic area and could assist decision-makers in conducting future risk assessments and formulating mitigation strategies in active volcanic regions, such as Nisyros.

**Supplementary Information** The online version contains supplementary material available at https://doi.org/10.1007/s00445-024-01779-9.

**Acknowledgements** Hersbach et al. (2018a,b) were downloaded from the Copernicus Climate Change Service (C3S) (2023). The results contain modified Copernicus Climate Change Service Material 2020. Neither the European Commission nor ECMWF is responsible for any use that may be made of the Copernicus Material or data it contains. We thank Roberto Sulpizio for his precious contribution in the conceptualization of this study. We thank Jacopo Natale for providing the high-resolution photogrammetric DEM used in Figs. 4, 5, and 6. A warm acknowledgement to Sideris for the precious welcome to his Coffee House during the period of the April 2023 gas survey.

**Funding** This research was supported by the HGME Sub-Project No. 2«Susceptibility estimation for Landslides in the Hellenic Territory – Volcanic Hazard and Risk Assessment—GEOKA» VOLCANIC SUSCEPTIBILITY ASSESSMENT OF THE HELLENIC TERRITORY. This study was carried out within the RETURN Extended Partnership and received funding from the European Union Next-GenerationEU (National Recovery and Resilience Plan – NRRP, Mission 4, Component 2, Investment 1.3 – D.D. 1243 2/8/2022, PE0000005). SM was also supported by the PON Research and Innovation 2014–2020 project referring to research contracts on green topics (grant no. CODICE CUP H95F21001440006). AC and GB were supported by the EU Horizon 2020 research and innovation program under grant agreement No 858092 (IMPROVE Project). GT was supported by MIUR, grant number project no. PRIN2017-2017LMNLAW "Connect4Carbon." This work is published with permission of the Executive Director of the British Geological Survey (UKRI).

**Data availability** Input files of numerical simulations and raw data of the local weather data and gas concentrations provided by the air quality stations are stored in the Supplementary Material.

**Code availability** DIAGNO model v.1.5.0 (Douglas et al. 1990) can be freely downloaded at http://datasim.ov.ingv.it/models/diagno.html.

DISGAS model v.2.6.0 (Costa and Macedonio 2016) can be freely downloaded at http://datasim.ov.ingv.it/models/disgas.html.

VIGIL workflow v.1.3.5 (Dioguardi et al. 2022) can be freely downloaded at https://github.com/BritishGeologicalSurvey/VIGIL.

## Declarations

**Competing interests** The authors declare no competing interests.

## References

Agency for Toxic Substances and Disease Registry (ATSDR) (1999) Toxicological profile for hydrogen sulfide. ATSDR, Atlanta, GA

Allard P, Carbonnelle J, Dajlevic D, Le Bronec J, Morel P, Robe MC, Maurenas JM, Faivre-Pierret R, Martin D, Sabroux JC, Zettwoog P (1991) Eruptive and diffuse emissions of $CO_2$ from Mount Etna. Nature 351:387–391

Allard V, Robin C, Newton PCD, Lieffering M, Soussana JF (2006) Short and long-term effects of elevated CO2 on Lolium perenne rhizodeposition and its consequences on soil organic matter turnover and plant N yield. Soil Biol Biochem 38(6):1178–1187

Arellano S, Yalire M, Galle B, Bobrowski A, Dingwell A, Johansson M, Norman P (2017) Long-term monitoring of $SO_2$ quiescent degassing from Nyiragongo's lava lake. J African Earth Sci 134:866–873

Auker MR, Sparks RSJ, Sieber L, Crosweller HS, Ewert J (2013) A statistical analysis of the global historical volcanic fatalities record. J Applied Volcanol 2:1–24

Badalamenti B, Liotta M, Valenza M (2001). An automatic system for continuous monitoring of $CO_2$, $H_2S$, $SO_2$ and meteorological parameters in the atmosphere of volcanic areas. Geochem Trans 5. https://doi.org/10.1039/B104622P

Baxter PJ (1990) Medical effects of volcanic eruptions: I. Main causes of death and injury. Bull of Volcanol 52:532–544

Baxter PJ, Kapila M (1989) Acute health impact of the gas release at Lake Nyos, Cameroon, 1986. J Volcanol Geotherm Res 39(2–3):265–275

Biagi R, Tassi F, Caliro S, Capecchiacci F, Venturi S (2022). Impact on air quality of carbon and sulfur volatile compounds emitted from hydrothermal discharges: the case study of Pisciarelli (Campi Flegrei, South Italy). Chemosphere 297. https://doi.org/10.1016/j.chemosphere.2022.134166

Biagi R, Ferrari M, Venturi S, Sacco M, Montegrossi G, Tassi F (2024) Development and machine learning-based calibration of low-cost multiparametric stations for the measurement of $CO_2$ and $CH_4$ in air. Heliyon 10(9):e29772. https://doi.org/10.1016/j.heliyon.2024.e29772

Bini G, Chiodini G, Cardellini C, Vougioukalakis GE, Bachmann O (2019) Diffuse emission of $CO_2$ and convective heat release at Nisyros caldera (Greece). J Volcanol Geotherm Res 376:44–53

Bini G, Chiodini G, Calir S, Tassi F, Vaselli O, Rizzo A, Mollo S, Vougioukalakis GE, Bachmann O (2022) Nitrogen, helium, and argon reveal the magmatic signature of fumarole gases and episodes of outgassing from upper-crustal magma reservoirs: the case of the Nisyros caldera (Aegean Arc, Greece). Geochim Cosmochim Acta 335:68–84

Boucher C, Lan T, Marty B, Burnard PG, Fischer TP, Ayalew D, Mabry J, Maarten de Moor J, Zelenski ME, Zimmermann L (2018) Atmospheric helium isotope composition as a tracer of volcanic emissions: a case study of Erta Ale volcano, Ethiopia. Chem Geol 480:3–11

Britter RE, McQuaid JD (1988). Workbook on the dispersion of dense gases, Technical report, HSE Contract Research Report No. 17/1988, Trinity Road Bootle, Merseyside L20 3QY, UK

Brombach T, Hunziker JC, Chiodini G, Cardellini C, Marini L (2001) Soil diffuse degassing and thermal energy fluxes from the southern Lakki Plain, Nisyros (Greece). Geophys Res Lett 28(1):69–72

Bussotti F, Bottacci A, Grossoni P, Mori B, Tani C (1997) Cytological and structural changes in Pinus pines L. needles following the application of an anionic surfactant. Plant Cell Environ 20(4):513–520

Caliro S, Chiodini G, Galluzzo D, Granieri D, La Rocca M, Saccorotti G, Ventura G (2005) Recent activity of Nisyros volcano (Greece) inferred from structural, geochemical and seismological data. Bull Volcanol 67:358–369

Caliro S, Viveiros F, Chiodini G, Ferreira T (2015) Gas geochemistry of hydrothermal fluids of the S. Miguel and Terceira Islands. Azores Geochimica Et Cosmochimica Acta 168:43–57

Carapezza ML, Badalamenti B, Cavarra L, Scalzo A (2003) Gas hazard assessment in a densely inhabited area of Colli Albani Volcano (Cava dei Selci, Roma). J Volcanol Geoth Res 123:81–94. https://doi.org/10.1016/S0377-0273(03)00029-5

Carapezza ML, Tarchini L, Ancona C, Forastiere F, Ranaldi M, Ricci T, De Simone G, Mataloni F, Pagliuca NM, Barberi F (2023) Health impact of natural gas emission at Cava dei Selci residential zone (metropolitan city of Rome, Italy). Environ Geochem Health 45(3):707–729

Cardellini C, Chiodini G, Frondini F (2003) Application of stochastic simulation to CO2 flux from soil: mapping and quantification of gas release. J Geophys Res 108(B9):2425

Cardellini C, Chiodini G, Frondini F, Avino R, Bagnato E, Caliro S, Lelli M, Rosiello A (2017) Monitoring diffuse volcanic degassing during volcanic unrests: the case of Campi Flegrei (Italy). Sci Rep 7(1):6757

Chiodini G, Cioni R, Leonis C, Marini L, Raco B (1993) Fluid geochemistry of Nisyros Island, Dodecanese. Greece J Volcanol Geotherm Res 56(1–2):95–112

Chiodini G, Cioni R, Guidi M, Raco B, Marini L (1998) Soil $CO_2$ flux measurements in volcanic and geothermal areas. Appl Geochem 13(5):543–552

Chiodini G, Avino R, Brombach T, Caliro S, Cardellini C, De Vita S, Frondini F, Granieri D, Marotta E, Ventura G (2004) Fumarolic and diffuse soil degassing west of Mount Epomeo, Ischia. Italy J Volcanol Geotherm Res 133(1–4):291–309

Chiodini G, Frondini F, Cardellin C, Granieri D, Marini L, Ventura G (2001) $CO_2$ degassing and energy release at Solfatara volcano, Campi Flegrei, Italy. J Geophys Res 106 (B8), 16: 213–16, 221

Chiodini G, Granieri D, Avino R, Caliro S, Costa A, Werner C (2005) Carbon dioxide diffuse degassing and estimation of heat release from volcanic and hydrothermal systems. J Geophys Res Solid Earth 110(B8)

Chiodini G, Baldini A, Barberi F, Carapezza ML, Cardellini C, Frondini F, Granieri D, Ranaldi M (2007) Carbon dioxide degassing at Latera caldera (Italy): evidence of geothermal reservoir and evaluation of its potential energy. J Geophys Res Solid Earth 112(B12)

Chiodini G (2009) $CO_2/CH_4$ ratio in fumaroles a powerful tool to detect magma degassing episodes at quiescent volcanoes. Geophys Res Lett 36(2)

Cihacek LJ, Bremner JM (1990) Capacity of soils for sorption of hydrogen sulfide. Comm in Soil Sci Plant Anal 21(5–6):351–363

Cortis A, Oldenburg CM (2009) Short-range atmospheric dispersion of carbon dioxide. Bound Lay Meteorol 133(1):17–34. https://doi.org/10.1007/s10546-009-9418-y

Costa A, Chiodini G (2015) Modelling air dispersion of $CO_2$ from limnic eruptions. Volcanic lakes. Springer, Berlin, Heidelberg, pp 451–465
Costa A, Folch A, Macedonio G (2013) Density-driven transport in the umbrella region of volcanic clouds: implications for tephra dispersion models. Geophys Res Lett 40(18):4823–4827
Costa A, Macedonio G (2016) DISGAS: a model for passive DISpersion of GAS. Rapporti tecnici INGV. 332. Istituto Nazionale Di Geofisica e Vulcanologia, Italy (2039e7941)
Costa A, Macedonio G, Chiodini G (2005) Numerical model of gas dispersion emitted from volcanic sources. Ann Geophys 48(4–5)
Cronin SJ, Sharp DS (2002) Environmental impacts on health from continuous volcanic activity at Yasur (Tanna) and Ambrym. Vanuatu, Int J Environm Health Res 12(2):109–123
Dietrich VJ, Lagios E (eds) (2017) Nisyros volcano: the Kos-Yali-Nisyros volcanic field. Springer
Dioguardi F, Massaro S, Costa A, Chiodini G, Folch A, Macedonio G, Sandri L, Selva J, Tamburello G (2022) VIGIL: a python tool for automatized probabilistic Volcanic Gas dIspersion modelLing. Ann Geophys 65(1):DM107. https://doi.org/10.4401/ag-8796
Douglas SG, Kessler RC, Carr EL (1990) User's guide for the Urban Airshed Model. Volume 3. User's manual for the Diagnostic Wind Model (No. PB-91–131243/XAB). Systems Applications, Inc., San Rafael, CA (USA)
Edmonds M, Grattan J, Michnowicz S (2018) Volcanic gases: silent killers. Observing the Volcano World: Volcano Crisis Communication 65–83
European Union (2009) Directive 2009/161/EU - indicative occupational exposure limit values. https://osha.europa.eu/en/legislation/directives/commission-directive-2009-161-eu-indicative-occupational-exposure-limit-values__;!!NLFGqXoFfo8MMQ!ttLq7IH4zL0kFCDX5tvdtBvPkpYIfJ380c3UjZtmNSLclggt2dbI8fMOujTolWzPSj6nTFZ0P9dYkQbh4rqyaShMc4L_Sg$
Folch A, Costa A, Hankin RKS (2009) TWODEE-2: a shallow layer model for dense gas dispersion on complex topography. Comput Geosci 35:667–674
Gagliano AL, Calabrese S, Daskalopoulou K, Cabassi J, Capecchiacci F, Tassi F, D'Alessandro W, (2019) Degassing and cycling of mercury at Nisyros volcano (Greece). Geofluids, ID 4783514, https://doi.org/10.1155/2019/4783514
Granieri D, Chiodini G, Marzocchi W, Avino R (2003) Continuous monitoring of $CO_2$ soil diffuse degassing at Phlegraean Fields (Italy): influence of environmental and volcanic parameters. Earth Planet Sci Lett 212(1–2):167–179
Guidotti TL (2010) Hydrogen sulfide: advances in understanding human toxicity. International J Toxicol 29(6):569–581
Hersbach H, Bell B, Berrisford P, Biavati G, Horányi A, Muñoz Sabater J, Nicolas J, Peubey C, Radu R, Rozum I, Schepers D, Simmons A, Soci C, Dee D, Thépaut JN (2018a) ERA5 hourly data on single levels from 1940 to present. Copernicus Climate Change Service (C3S) Climate Data Store (CDS). https://doi.org/10.24381/cds.adbb2d47. Accessed on 30–12–2023
Hersbach H, Bell B, Berrisford P, Biavati G, Horányi A, Muñoz Sabater J, Nicolas J, Peubey C, Radu R, Rozum I, Schepers D, Simmons A, Soci C, Dee D, Thépaut JN (2018b) ERA5 hourly data on pressure levels from 1940 to present. Copernicus Climate Change Service (C3S) Climate Data Store (CDS). https://doi.org/10.24381/cds.adbb2d47. Accessed on 30–12–2023
Kern C, Lerner AH, Elias T, Nadeau PA, Holland L, Kelly PJ, Werner CA, Clor LE, Cappos M (2020) Quantifying gas emissions associated with the 2018 rift eruption of Kīlauea volcano using ground-based DOAS measurements. Bull Volcanol 82(7):55
Kristmannsdóttir H, Sigurgeirsson M, Ármannsson H, Hjartarson H, Ólafsson M (2000) Sulfur gas emissions from geothermal power plants in Iceland. Geothermics 29(4–5):525–538
Lambert TW, Goodwin VM, Stefani D, Strosher L (2006) Hydrogen sulfide ($H_2S$) and sour gas effects on the eye. A historical perspective.Sci Total Environ 367(1):1–22
Linhares D, Garcia PV, Viveiros F, Ferreira T, Rodrigues ADS (2015) Air pollution by hydrothermal volcanism and human pulmonary function. Biomed Res Int 2015(1):326794
Marini L, Principe C, Chiodini G, Cioni R, Fytikas M, Marinelli G (1993) Hydrothermal eruptions of Nisyros (Dodecanese, Greece). Past events and present hazard. J Volcanol Geotherm Res 56:71–94
Marini L, Fiebig J (2005) Fluid geochemistry of the magmatic-hydrothermal system of Nisyros (Greece)
Massaro S, Stocchi M, Tamburello G, Costa A, Sandri L, Caliro S, Chiodini G, Selva J, Dioguardi F, Folch A (2022) Validating gas dispersion modelling at La Solfatara (Campi Flegrei, South Italy). Nuovo Cimento Soc Ital Fis C 45(6):186
Massaro S, Dioguardi F, Sandri L, Tamburello G, Selva J, Moune S, Jessop DE, Moretti R, Komorowski JC, Costa A (2021) Testing gas dispersion modelling: a case study at La Soufrière volcano (Guadeloupe, Lesser Antilles). J Volcanol Geotherm Res 417. https://doi.org/10.1016/j.jvolgeores.2021.107312
Montegrossi G, Tassi F, Vaselli O, Buccianti A, Garofalo K (2001) Sulfur species in volcanic gases. Anal Chem 73(15):3709–3715. https://doi.org/10.1021/ac001429b
Olafsdottir S, Gardarsson SM, Andradottir HO (2014) Natural near field sinks of hydrogen sulfide from two geothermal power plants in Iceland. Atm Environm 96:236–244
Papadopoulos GA, Sachpazi M, Panopoulou G, Stavrakakis G (1998) The volcanoseismic crisis of 1996–97 in Nisyros, SE Aegean Sea, Greece. Terra Nova 10:151–154
Pebesma EJ (2004) Multivariable geostatistics in S: the gstat package. Comput Geosci 30(7):683–691
Pecoraino G, Scalici L, Avellone G, Ceraulo L, Favara R, Candela EG, Scaletta C (2008) Distribution of volatile organic compounds in Sicilian groundwaters analysed by head space-solid phase micro extraction coupled with gas chromatography mass spectrometry (SPME/GC/MS). Water Res 42(14):3563–3577
Popa RG, Bachmann O, Ellis BS, Degruyter W, Tollan P, Kyriakopoulos K (2019) A connection between magma chamber processes and eruptive stylesrevealed at Nisyros-Yali volcano (Greece). J Volcanol Geoth Res 387:106666
Popa RG, Guillong M, Bachmann O, Szymanowski D, Ellis B (2020) U-Th zircondating reveals a correlation between eruptive styles and repose periods at the Nisyros-Yali volcanic area, Greece. Chem Geol 555:119830
R Core Team (2023) R: a language and environment for statistical computing_. R Foundation for Statistical Computing,Vienna, Austria. https://www.R-project.org/
Rafflin V, Boudoire G, Massaro S, Stocchi M, Costa Grassa F, Giuffrida G, Gailler L, Liuzzo M, Planche C, Banson S, Harris A (2024) Modelling $CO_2$ dispersion in the air during potential limnic eruption at the lake Pavin (France). J Volcanol Geoth Res 447:108024
Rickard D, Luther GW (2007) Chemistry of iron sulfides. Chem Rev 107(2):514–562
Santana MC, Weir A, Rumbeiha WK (2022) A comprehensive review of treatments for hydrogen sulfide poisoning: past, present, and future. Toxicol Mech Methods 33(3):183–196. https://doi.org/10.1080/15376516.2022.2121192
State of Hawaii (2002) Report on hazard evaluation and emergency response office activities for FY 2001. Department of Health, State of Hawaii
Stewart C, Damby DE, Horwell CJ, Elias T, Ilyinskaya E, Tomašek I, Longo BM, Schmidt A, Carlsen HK, Mason E, Baxter PJ, Cronin S, Witham C (2022) Volcanic air pollution and human health: recent advances and future directions. Bull Volcanol 84(1):11

Symonds RB (1994) Volcanic-gas studies: methods, results, and applications, in Volatiles in magma. Rev Mineral 30:1–66
Symonds RB, Gerlach TM, Reed MH (2001) Magmatic gas scrubbing: implications for volcano monitoring. J Volcanol Geoth Res 108(1–4):303–341
Tamburello G (2015) Ratiocalc: software for processing data from multicomponent volcanic gas analyzers. Comput Geosci 82:63–67
Thorsteinsson T, Hackenbruch J, Sveinbjörnsson E, Jóhannsson T (2013) Statistical assessment and modeling of the effects of weather conditions on $H_2S$ plume dispersal from Icelandic geothermal power plants. Geothermics 45:31–40
Tibaldi A, Pasquare FA, Papanikolaou D, Nomikou P (2008) Tectonics of Nisyros Island, Greece, by field and offshore data, and analogue modelling. J Struct Geol 30(12):1489–1506
Toutain JP, Baubron JC, François L (2002) Runoff control of soil degassing at an active volcano. The case of Piton de la Fournaise, Réunion Island. Earth Planet Sci Lett 197(1–2):83–94
U.S. Environmental Protection Agency (U.S.EPA) (2003) IRIS record for hydrogen sulfide. https://iris.epa.gov/static/pdfs/0061_summary.pdf
van Manen SM (2014) Perception of a chronic volcanic hazard: persistent degassing at Masaya volcano. Nicaragua J Applied Volcanol 3(1):1–16
Vaselli O, Tassi F, Giannini L, Capaccioni B, Montegrossi G (2006) Sampling and analysis of volcanic gases. Sampling and Analysis of Volcanic Gases 1000–1012
Viveiros F, Cardellini C, Ferreira T, Silva C (2012) Contribution of $CO_2$ emitted to the atmosphere by diffuse degassing from volcanoes: the Furnas Volcano case study. Intern J Global Warm 4(3–4):287–304
Viveiros F, Baldoni E, Massaro S, Stocchi M, Costa A, Caliro S, Chiodini G, Andrade C (2023) Quantification of $CO_2$ degassing and atmospheric dispersion at Caldeiras da Ribeira Grande (São Miguel Island, Azores). J Volcanol Geotherm Res 438:107807
Vougioukalakis G (1993) Volcanic stratigraphy and evolution of Nisyros Island. Bull Geol Soc Greece 28(2):239–258
Watson AJ, Lovelock JE, Margulis L (1978) Methanogenesis, weathering and the regulation of atmospheric oxygen. Nature 272:189–192. https://doi.org/10.1038/272189a0
Watts SF (2000) The mass budgets of carbonyl sulfide, dimethyl sulfide, carbon disulfide and hydrogen sulfide. Atm Environm 34(5):761–779
Williams-Jones G, Rymer H (2015) Hazards of volcanic gases. In: The encyclopedia of volcanoes. Academic Press, pp 985–992
World Health Organization (2000) Air quality guidelines for Europe, 2nd edn. World Health Organization, Regional Office for Europe
World Health Organization (1981) Disability prevention and rehabilitation: report of the WHO Expert Committee on Disability Prevention and Rehabilitation [meeting held in Geneva from 17 to 23 February 1981]